Inorganic Chemistry
Article

Inorg. Chem. **2009**, *48*, 11187–11195 **11187**
DOI: 10.1021/ic901607u

2-Thienylcarboxylato and 2-Thienylthiocarboxylato Ligands Bonded to MM Quadruple Bonds (M = Mo or W): A Comparison of Ground State, Spectroscopic and Photoexcited State Properties

Brian G. Alberding, Malcolm H. Chisholm,* Yi-Hsuan Chou, Yagnaseni Ghosh, Terry L. Gustafson,* Yao Liu, and Claudia Turro*

Department of Chemistry, The Ohio State University, 100 W. 18th Avenue, Columbus, Ohio 43210

Received August 11, 2009

The compounds $M_2(TiPB)_2(OSC\text{-}2\text{-}Th)_2$ have been prepared from the reactions between $M_2(TiPB)_4$ and Th-2-COSH (2 equiv) in toluene solution, where M = Mo (**Mo_2ThCOS**) or W (**W_2ThCOS**), TiPB = 2,4,6-triisopropylbenzoate and Th = thienyl. The molybdenum and tungsten compounds are pink and blue, air-sensitive, ether soluble solids that show M^+ ions in the mass spectrometer and metal and ligand based reversible oxidation and reduction waves, respectively, by cyclic voltammetry. Electronic structure calculations on the model compounds $M_2(O_2CH)_2(OSC\text{-}2\text{-}Th)_2$ indicate that the highest occupied molecular orbital (HOMO) is principally $M_2\delta$ and the lowest unoccupied molecular orbital (LUMO) is thienylthiocarboxylate π^* but with significant metal−sulfur mixing. The intense visible absorptions arise from ^{1}MLCT, $M_2\delta$ to thienylthiocarboxylate. The photoexcited states of these molecules have been studied by transient absorption spectroscopy and steady state emission. These properties are compared with those of previously reported thienylcarboxylate compounds, $M_2(TiPB)_2(O_2C\text{-}2\text{-}Th)_2$, where M = Mo (**$Mo_2ThCO_2$**) or W (**$W_2ThCO_2$**).

Introduction

The classification of ligands and metals as being hard or soft is perhaps most useful at the extreme left and right-hand side of the d-block elements.[1] Thus, the group 4 and 5 elements can easily be seen as hard metals and oxophilic while the group 10, 11, and 12 metals are soft having relatively little affinity toward oxygen but a greater affinity toward sulfur. In the middle of the d-block the classification is less clear-cut and may rest with the specific oxidation state of the metal and the nature of the ancillary ligands. Certainly, this could be claimed for molybdenum and tungsten which in their high oxidation states of +5 and +6 can be claimed to be oxophilic and hard but in their lower oxidation states of 0 and +2 can be considered soft with a high affinity for tertiary phosphines and other soft π-acceptor ligands. In our studies of the chemistry of MM (M = Mo or W) multiply bonded complexes of molybdenum and tungsten, we have compared the influence of alkoxide and thiolate ligands on the electronic structure and reactivity of the triply bonded ethane-like dimers $X_3M{\equiv}MX_3$.[2] Here the stronger π-donating properties of the alkoxide labilize the M≡M bond toward reactions with π-acceptor ligands such as CO, alkynes, and nitriles leading in certain cases to reductive cleavage reactions.[3] In our studies of linked MM quadruple bonds we have shown that the electronic coupling by thioterephthalate bridges $[SOCC_6H_4COS]^{2-}$ is much larger in comparison to terephthalate $[O_2CC_6H_4CO_2]^{2-}$.[4] The principal origin of this phenomenon lies in the lower energy of the C−S π^* orbital which affords greater $M_2\delta$ to bridge π^* back-bonding. However, there is also a secondary reason which arises from the weaker C−S π bond and the higher energy of the sulfur 3p π atomic orbital relative to its oxygen counterpart. This leads to a greater mixing of the S 3p orbital with the out-of-phase combination of the filled $M_2\delta$ orbitals which is the highest occupied molecular orbital (HOMO) of the bridged complexes. We were naturally led to question what effect the substitution of a sulfur for an oxygen would have at a *trans*-disubstituted compound of the type $M_2(TiPB)_2(O_2C\text{-}L)_2$ shown in Figure 1, where TiPB = 2,4,6-triisopropylbenzoate.

Here the bulky TiPB ligands are trans and their C_6 rings are twisted out of the $-O_2C$ plane removing $M_2\delta$ to arene π-conjunction. $(O_2C\text{-}L)\pi\text{-}M_2\delta\text{-}(O_2C\text{-}L)\pi$ conjugation arises principally from the interaction of the out-of-phase carboxylate π^* combination shown in Figure 2 and is maximized when the aromatic rings are coplanar with the carboxylate planes. This is indeed seen in the solid state structures where

*To whom correspondence should be addressed. chisholm@chemistry.ohio-state.edu (M.H.C.), gustafson@chemistry.ohio-state.edu (T.L.G.), turro@chemistry.ohio-state.edu (C.T.).

(1) Pearson, R. G. *J. Am. Chem. Soc.* **1963**, *85*, 3533.
(2) Chisholm, M. H.; Davidson, E. R.; Huffman, J. C.; Quinlan, K. B. *J. Am. Chem. Soc.* **2001**, *123*, 9652.
(3) Chisholm, M. H. *Chem. Rec.* **2001**, *1*, 12.
(4) Chisholm, M. H.; Patmore, N. J. *Dalton Trans.* **2006**, 3164.

Published on Web 11/04/2009

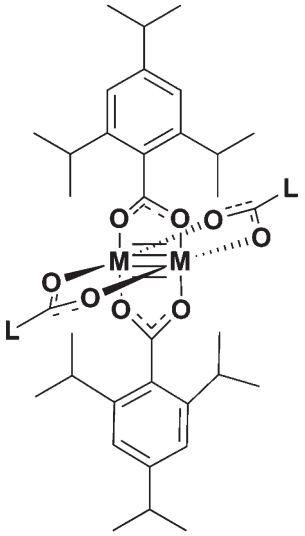

Figure 1. Generic structure of a *trans*-$M_2(TiPB)_2(O_2C\text{-}L)_2$ compound, where M = Mo or W.

L = 6-azulene,[5] 2-thiophene[6] and 2,2′-bithiophene.[7] By symmetry the non-bonding carboxylate lone pair orbitals can interact with the MMδ*, but the energy difference makes this interaction of little significance. Here we report the preparation of the new compounds *trans*-$M_2(TiPB)_2(OSC\text{-}2\text{-}Th)_2$, where M = Mo(**$Mo_2$ThCOS**) or W(**$W_2$ThCOS**), Th = thienyl, and compare their properties with the previously reported $M_2(TiPB)_2(O_2C\text{-}2\text{-}Th)_2$ compounds, where M = Mo (**Mo_2ThCO$_2$**)[7] or W(**W_2ThCO$_2$**).[6]

Results and Discussion

Syntheses. The new ligand Th-2-COSH and the compounds **Mo_2ThCOS** and **W_2ThCOS**, were prepared according to the reactions shown in Scheme 1. Details are described in the Experimental Section. **Mo_2ThCOS** is pink and **W_2ThCOS** is blue. Both compounds are air and moisture-sensitive. They are sparingly soluble in hexane and toluene but appreciably soluble in tetrahydrofuran (THF). They showed molecular ions M^+ by matrix assisted laser desorption/ionization time-of-flight (MALDI-TOF) mass spectrometry and gave satisfactory elemental analysis. The ^{1}H NMR spectra are consistent with the *trans*-substitution pattern (for *cis*-substitution, we would expect the isopropylmethyl groups of TiPB ligands to reveal diastereotopism). Compounds **Mo_2ThCO$_2$** and **W_2ThCO$_2$** were prepared according to reported procedures.[6]

Solid-State Molecular Structure. Single crystals of **Mo_2ThCOS** grown from THF solutions were examined, and a partial solution was obtained. The refinement was complicated by a disorder of the sulfur atoms both within the thienyl ring and the −OSC moiety, and a satisfactory solution was not obtained. This notwithstanding, the gross structural features are akin to that of its thienyl carboxylate analogue, **Mo_2ThCO$_2$**,[6] as depicted in the drawing in Supporting Information, Figure S1.

Electronic Absorption Spectroscopy. The UV−vis electronic absorption spectra for the compounds are shown in Figure 3. Two notable features are immediately obvious in relation to the lowest energy ^{1}MLCT bands.

(1) The spectra of the ditungsten compounds, **W_2ThCOS** and **W_2ThCO$_2$**, are red-shifted compared to their dimolybdenum counterparts, **Mo_2ThCOS** and **Mo_2ThCO$_2$**, respectively. This is consistent with the relative energies of the $M_2\delta$ orbitals and is in-line with both electrochemical measurements and computations (vide infra). (2) The ^{1}MLCT bands of **Mo_2ThCOS** and **W_2ThCOS** are red-shifted compared to **Mo_2ThCO$_2$ and W_2ThCO$_2$**, respectively. This indicates that the substitution of S for O in the $-O_2C$ moiety has a pronounced influence in lowering the energy of the ^{1}MLCT transition, the $M_2\delta$ to thienyl π* transition. At higher energies and $\lambda_{max} \sim 400$ nm for **W_2ThCOS** and **W_2ThCO$_2$** and ~320 nm for **Mo_2ThCOS** and **Mo_2ThCO$_2$** compounds there is a weaker absorption due to $M_2\delta$ to $-O_2C$ π* of the TiPB ligands. This transition is similarly seen in the parent $M_2(TiPB)_4$ compounds, albeit, that they are more red-shifted because of greater coplanarity of the TiPB ligands with the dimetal core in the parent $M_2(TiPB)_4$ compounds.[8] In all cases the ^{1}MMδ to δ* transition, which is known to be weak with, $\varepsilon \sim 100$ $M^{-1}cm^{-1}$, and is expected to occur around $\lambda_{max} \sim 460$ nm, is masked by the intense ^{1}MLCT. Finally, it can be noted that there are absorptions at < 300 nm which we assign to aromatic ring (TiPB) π to π* transitions, ^{1}LC. The relative intensities of the ^{1}MLCT bands follow the order $Mo_2 < W_2$ and $O_2C <$ OSC as expected for MLCT bands which to a first order approximation correlate with the energy difference between the two states. In Figure 3, the spectra are drawn to a normalized intensity scale such that all ^{1}MLCT bands have equivalent intensities. That the room temperature solution ^{1}MLCT absorption of the tungsten compounds, **W_2ThCO$_2$** and **W_2ThCOS**, show vibronic features is also worthy of note. On lowering the temperature, these become more pronounced, as shown for **W_2ThCO$_2$** in Supporting Information, Figure S2. This most likely reflects the greater degree of $M_2\delta$ to ligand π* back-bonding and the higher barrier to rotation about the C−C bond of the O_2C/OSC-Th ring. At low temperature the Boltzmann distribution of rotamers about the C−C bond of the O_2C/OSC-Th ring planes favor the planar geometry. A more detailed discussion of vibronic features and the nesting of the potential energy surfaces in ^{1}MLCT transitions is given in a recent paper.[9]

Luminescence Studies. Both **Mo_2ThCO$_2$** and **Mo_2ThCOS** show evidence of weak fluorescence from their ^{1}MLCT states at ~560 and ~620 nm, respectively, and **W_2ThCO$_2$** also shows weak ^{1}MLCT emission at ~700 nm, as shown in Figure 4. Because of the limits of our instrumentation (one detector cuts off at > 800 nm) we are not able to detect any emission from the ^{1}MLCT state of the thienylthiocarboxylate of tungsten, **W_2ThCOS**.

(5) Barybin, M. V.; Chisholm, M. H.; Patmore, N. J.; Robinson, R. E.; Singh, N. *Chem. Commun.* **2007**, 3652.
(6) Chisholm, M. H.; Epstein, A. J.; Gallucci, J. C.; Feil, F.; Pirkle, W. *Angew. Chem., Int. Ed.* **2005**, *44*, 6537.
(7) Burdzinski, G. T.; Chisholm, M. H.; Chou, P. T.; Chou, Y. H.; Feil, F.; Gallucci, J. C.; Ghosh, Y.; Gustafson, T. L.; Ho, M. L.; Liu, Y.; Ramnauth, R.; Turro, C. *Proc. Natl. Acad. Sci. U.S.A.* **2008**, *105*, 15247.
(8) Alberding, B. G.; Chisholm, M. H.; Chou, Y.-H.; Gallucci, J. C.; Ghosh, Y.; Gustafson, T. L.; Patmore, N. J.; Reed, C. R.; Turro, C. *Inorg. Chem.* **2009**, *48*, 4394.
(9) Lear, B. J., Chisholm, M. H. *Inorg. Chem.*, published ASAP October 27, 2009 (ic900995u).

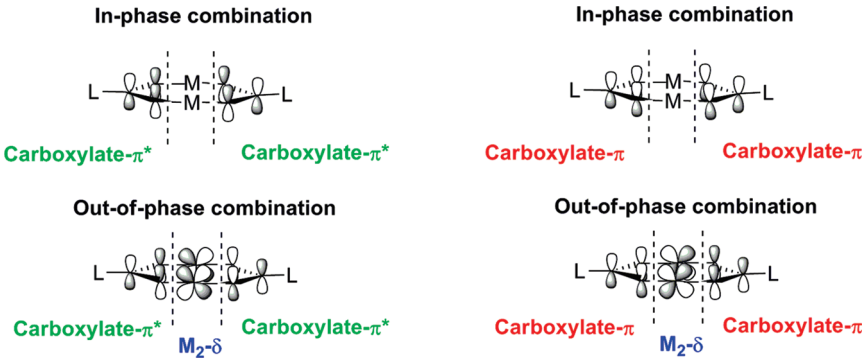

Figure 2. Orbital interactions between filled M_2-δ and empty carboxylate π^* and filled carboxylate π orbitals.

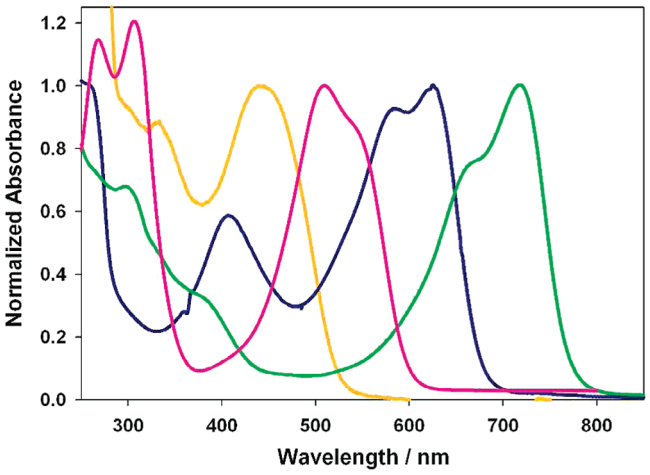

Figure 3. UV−vis absorption spectra of $M_2(TiPB)_2(OXC\text{-}2\text{-}Th)_2$compounds; orange for $\mathbf{Mo_2ThCO_2}$; pink for $\mathbf{Mo_2ThCOS}$; blue for $\mathbf{W_2ThCO_2}$; and green for $\mathbf{W_2ThCOS}$.

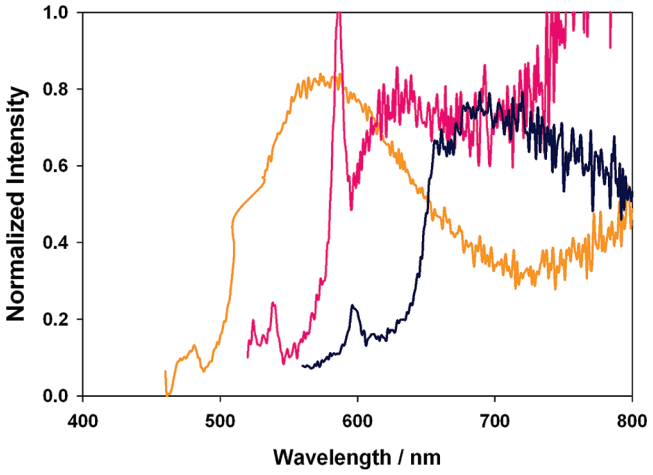

Figure 4. Emission spectra of $M_2(TiPB)_2(OXC\text{-}2\text{-}Th)_2$ compounds at room temperature; orange for $\mathbf{Mo_2ThCO_2}$ with λ_{ex} = 450 nm; pink for $\mathbf{Mo_2ThCOS}$ with λ_{ex} = 550 nm; blue for $\mathbf{W_2ThCO_2}$ with λ_{ex} = 560 nm.

Scheme 1. Synthesis of Th-2-COSH Ligand and $M_2(TiPB)_2(OSC\text{-}2\text{-}Th)_2$ Compounds

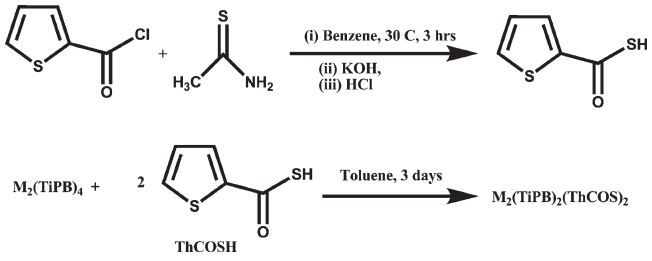

For all four compounds mentioned, excitation spectra for the singlet emission indicated that the emissions arise from the compounds and not from any impurities. With a NIR detector that operates in the range 800−1600 nm, we observed strong room temperature phosphorescence for both $\mathbf{Mo_2ThCO_2}$ and $\mathbf{Mo_2ThCOS}$; at ∼1100 nm and at 77 K these show vibronic features due to υ(Mo−Mo) ∼ 400 cm^{-1} as shown in Supporting Information, Figure S3 for $\mathbf{Mo_2ThCOS}$. On the basis of earlier reports on related compounds,7,8,10 we assign these emissions as arising from the $^3MM\delta\delta^*$ state. A triplet emission at ∼1070 nm is also observed for the tungsten compound, $\mathbf{W_2ThCO_2}$. A recent report from our lab has shown, that, the $^3WW\delta\delta^*$ based emission has its λ_{max} at ∼820 nm and exhibits prominent vibronic features of ∼390 cm^{-1} attributable to a υ(WW) stretching. On the basis of the energy of λ_{max} of triplet emission for $\mathbf{W_2ThCO_2}$ and absence of aforementioned vibronic spacings in the emission peak, we assign the emissive state to be a ^{3}MLCT state.

For $\mathbf{W_2ThCOS}$ we see very weak near-infrared (NIR) emission only at low temperature (77 K), centered at ∼1090 nm, which we assign to be arising from the ^{3}MLCT state, using the same arguments as used for $\mathbf{W_2ThCO_2}$. The NIR emission spectra for the three emissive compounds are shown in Figure 5.

At this point it is worth noting that although the substitution of S for O leads to a significant red shift for the ^{1}MLCT absorption, the triplet emission for the tungsten compounds, $\mathbf{W_2ThCOS}$ and $\mathbf{W_2ThCO_2}$, occurs at a similar energy. The Stoke's shift for the compounds $\mathbf{W_2ThCOS}$ and $\mathbf{W_2ThCO_2}$ for singlet absorption and triplet emission are 4600 and 6650 cm^{-1}, respectively. A similar effect is seen for the molybdenum compounds where the Stokes shift of the ^{1}MLCT absorption and S_1 emissive states are 2500 and 4680 cm^{-1} for the −OSC and $-O_2C$ containing compounds, $\mathbf{Mo_2ThCOS}$ and $\mathbf{Mo_2ThCO_2}$, respectively.

Hence, we see that energy and character of the photoexcited states depend on the metal center (Mo or W) as well as on the heteroatom X in the co-ordinating −OXC

(10) Chisholm, M. H.; Chou, P.-T.; Chou, Y.-H.; Ghosh, Y.; Gustafson, T. L.; Ho, M.-L. *Inorg. Chem.* **2008**, *47*, 3415.

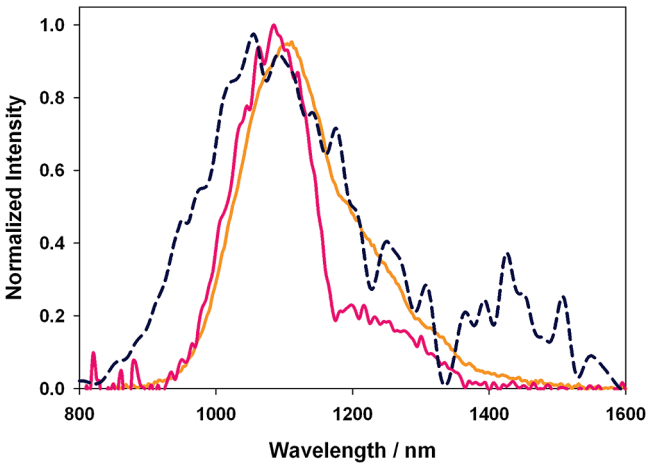

Figure 5. NIR emission spectra for $M_2(TiPB)_2(OXC\text{-}2\text{-}Th)_2$ compounds at room temperature; where orange for $\mathbf{Mo_2ThCO_2}$ with λ_{ex} = 405 nm; pink for $\mathbf{Mo_2ThCOS}$ with λ_{ex} = 532 nm; and blue for $\mathbf{W_2ThCO_2}$ with λ_{ex} = 675 nm.

Table 1. Oxidation and Reduction Potentials for $M_2(TiPB)_2(OXC\text{-}2\text{-}Th)_2$ Compounds, Where M = Mo or W and X = O or S, in THF, versus $Cp_2Fe^{0/+}$ Couple

compounds	oxidation potential (V)	reduction potential 1 (V)
$Mo_2(TiPB)_2(OSC\text{-}2\text{-}Th)_2$	0.16	−2.38
$W_2(TiPB)_2(OSC\text{-}2\text{-}Th)_2$	−0.32	−2.25
$Mo_2(TiPB)_2(O_2C\text{-}2\text{-}Th)_2$	0.056	−2.88
$W_2(TiPB)_2(O_2C\text{-}2\text{-}Th)_2$	−0.56	−2.81

functionality. $\mathbf{Mo_2ThCOS}$ and $\mathbf{Mo_2ThCO_2}$ indicate the presence of two emissive states, ^{1}MLCT and ^{3}MM$\delta\delta^*$. The two ditungsten compounds, $\mathbf{W_2ThCOS}$ and $\mathbf{W_2ThCO_2}$, also indicate the presence of weakly emitting photoexcited states, a higher energy ^{1}MLCT and a lower energy ^{3}MLCT state.

Electrochemical Studies. The electrochemical properties of the four compounds were examined in THF by both cyclic voltammetry and differential pulse voltammetry. A summary of redox potentials relative to the $Cp_2Fe^{0/+}$ couple is given in Table 1. All compounds show reversible oxidation waves that can readily be assigned to the removal of an electron from the $M_2\delta$ orbital. That it is easier to oxidize the W_2- relative to the Mo_2-containing compounds is consistent with the expected relative $M_2\delta$ orbital energies. This is also seen in the parent $M_2(TiPB)_4$ compounds.[8] However, that it is easier to oxidize the carboxylate compounds, $\mathbf{Mo_2ThCO_2}$ and $\mathbf{W_2ThCO_2}$, by >200 mV relative to the thiocarboxylate compounds, $\mathbf{Mo_2ThCOS}$ and $\mathbf{W_2ThCOS}$, respectively, is perhaps less expected and certainly noteworthy. It implies that the substitution of S for an O, in the $-O_2C$ functionality, stabilizes the $M_2\delta$ orbital, and this is supported by electronic structure calculations (vide infra). The compounds also show reduction waves associated with reduction of the thienyl ligands. This is equivalent to putting an electron in the empty thienyl ligand based π^* orbital, the lowest unoccupied molecular orbital (LUMO). The first reduction becomes easier on going from $\mathbf{Mo_2ThCO_2}$ to $\mathbf{Mo_2ThCOS}$ and from $\mathbf{W_2ThCO_2}$ to $\mathbf{W_2ThCOS}$. This implies that the thienyl ligand based π^* orbital gets stabilized upon substitution of an O with S in the $-O_2C$

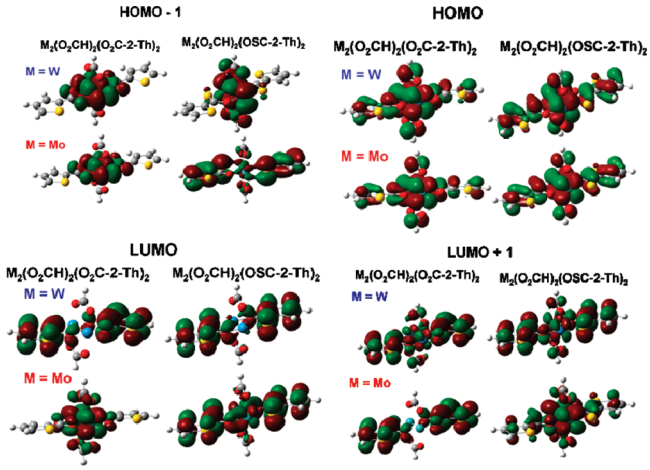

Figure 6. Gaussview plots of frontier orbitals drawn with iso-surface value = 0.02 for $M_2(O_2CH)_2(XOC\text{-}2\text{-}Th)_2$compounds, where, M = Mo or W and X = O or S.

functionality. This trend is reflected in the energies of the LUMOs as obtained from electronic structure calculations (vide infra). Additionally, $\mathbf{Mo_2ThCOS}$ clearly shows two reduction waves separated by 320 mV.

Electronic Structure Calculations. To obtain a more quantitative insight into the bonding, spectroscopies, and electrochemical data of these compounds, we carried out electronic structure calculations employing density functional theory (DFT).[11−14] In these calculations formate ligands were substituted for the TiPB ligands, and the model compounds were thus *trans*-$M_2(O_2CH)_2(OXC\text{-}2\text{-}Th)_2$, where M = Mo or W and X = O or S. Because of the large dihedral angle involving the C_6 ring and the $-O_2C$ groups of the TiPB plane, there is relatively little $M_2\delta$ to TiPB back-bonding, so these model compounds, with formates as ancillary groups, allow us to interrogate the nature of the $M_2\delta$-thienylcarboxylate and thienylthiocarboxylate bonding. Calculations were carried out on six possible geometries of the model compounds, *trans*-$M_2(O_2CH)_2(OXC\text{-}2\text{-}Th)_2$. These are depicted in Supporting Information Figure S4, which shows six different ways of *trans*-orientation of the $ThCOS^-$ ligands about the MM quadruple bond. The highest energy geometry was C_s while the lowest energy geometry was C_{2h} and the energy difference between these two conformers is only 0.22 kJ/mol. These small energy differences between the various ground state geometries imply there will be very little difference in the nature and energy of the frontier orbitals among the various conformers. That is why the lowest energy geometry of C_{2h} was chosen when further calculations were performed.

Gaussview[15] plots of the respective HOMO, HOMO−1, LUMO, and LUMO+1 orbitals are shown in Figure 6 and these, together with the frontier molecular orbital

(11) Hohenberg, P.; Kohn, W. *Phys. Rev.* **1964**, 164.
(12) Kohn, W.; Sham, L. J. *Phys. Rev.* **1965**, *137*, 1697.
(13) Parr, R. G.; Yang, W. *Density-functional Theory of Atoms and Molecules*; Oxford University Press: New York, 1989; p 333 ff.
(14) *The Challenge of d and f Electrons: Theory and Computation*; Salahub, D. R., Zerner, M. C., Eds.; ACS Symposium Series 394; Developed from a Symposium at the 3rd Chemical Congress of North America Toronto, Canada, June 5−11, 1988; American Chemical Society: Washington, DC, 1989; p 405 ff.
(15) Dennington, R., II; Keith, T.; Millam, J.; Eppinnett, K.; Hovell, W. L.; Gilliland, R. *GaussView*; Semichem Inc: Shawnee Mission, KS, 2003.

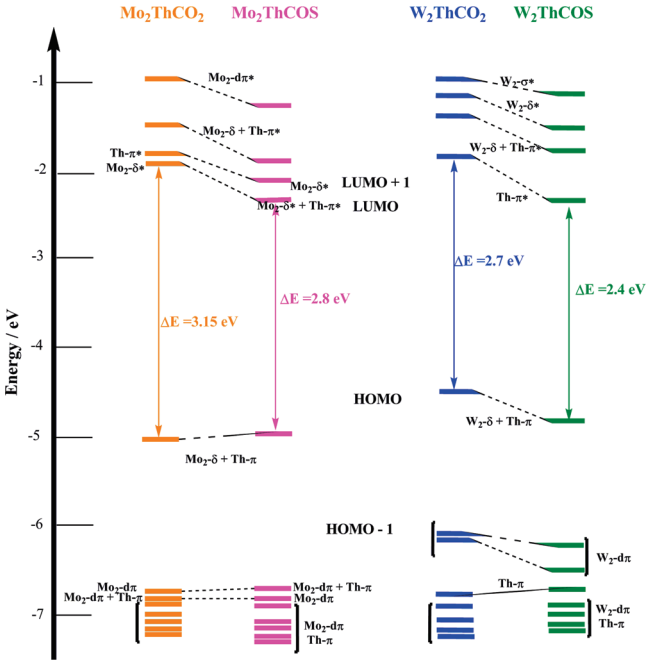

Figure 7. Orbital energy level diagram for $M_2(O_2CH)_2(OXC\text{-}2\text{-}Th)_2$ model compounds, where, M = Mo or W and X = O or S.

energy level diagram shown in Figure 7, reveal some very interesting features.

The HOMO is in all cases the $M_2\delta$ orbital. The HOMO-1 and HOMO-2 are MMπ bonding orbitals for both tungsten complexes, whereas, for **Mo_2ThCOS**, the HOMO-1 and HOMO-3 are in- and out-of-phase combinations of filled thienylthiocarboxylate π orbitals and the HOMO-2 is a MMπ orbital. For **Mo_2ThCO$_2$**, the HOMO-1 and HOMO-2 are MMπ bonding orbitals (see Supporting Information, Figure S5 for additional frontier orbitals for the $M_2(O_2CH)_2(COX\text{-}2\text{-}Th)_2$ compounds).

An examination of the energy levels of the frontier molecular orbitals, as depicted in Figure 7, reveals that the substitution of S for O in the $-O_2C$ functionality causes the energy levels of the HOMO, HOMO-1, and HOMO-2 to remain essentially the same in the molybdenum compounds. However, in the tungsten compounds this substitution leads to lowering of the energies and consequent stabilization of the aforementioned orbitals. This stabilization of the HOMO was reflected in the experimentally observed oxidation potentials of the compounds.

For the tungsten compounds, the LUMO and the LUMO+1 are respectively the in-phase and out-of-phase combinations of the lowest energy π^* orbitals of the thienylcarboxylate and thiocarboxylato ligands and the energy splitting of these is a measure of the $W_2\delta$ to ligand π^* interaction. As can be seen in Figure 6, the LUMO+1 contains some contribution from the $M_2\delta$.

For molybdenum, the LUMO is the $M_2\delta^*$ based orbital for **Mo_2ThCO$_2$** but ligand π^* based for **Mo_2ThCOS**, with some admixture from $Mo_2\delta^*$. The LUMO+1 is mostly $Mo_2\delta^*$ for the thiocarboxylate and ligand π^* for the carboxylate.

Going back to Figure 7, we see that the energies of the LUMO and LUMO+1 orbitals are lowered for both molybdenum and tungsten compounds when one O in the $-O_2C$ functionality is replaced with S. This stabilization effect on the thienyl π^* based orbitals was again reflected in the reduction potentials of the compounds. The calculations thus support the observed trends seen in the metal based oxidation and the thienyl based reduction potentials and also in the trends seen for the ^{1}MLCT bands. These subtle differences in energies of the frontier orbitals between molybdenum and tungsten arise because of the relative orbital energies of the $M_2\delta$ to $-$OSC π system. In the case of molybdenum the enhanced backbonding, $M_2\delta$ to $-$OSC π^*, is more than compensated by the S 3p to Mo_2 δ filled$-$filled interaction with the net result that the $Mo_2\delta$ is slightly raised in energy relative to the $-O_2C$ complex. However, for tungsten, the higher energy of the $W_2\delta$ orbital is further removed in energy from the filled S 3pπ orbital and closer to the $-$OSCπ^* orbital. Here the greater $W_2\delta$ to $-$OSC π^* backbonding leads to a stabilization of the $W_2\delta$ relative to the $-O_2C$ analogue.

Table 2. Lifetimes of Singlet and Triplet Excited States Determined from fs and ns TA Spectroscopic Measurements

compounds	$\tau_{^1\text{MLCT}}$ (ps)	$\tau_{^3\text{MM}\delta\delta^*}$ (μs)	$\tau_{^3\text{MLCT}}$ (ns)
$Mo_2(TiPB)_2(OSC\text{-}2\text{-}Th)_2$	1.99 ± 0.06[a]	51[b]	
$Mo_2(TiPB)_2(O2C\text{-}2\text{-}Th)_2$	4.1[c]	77[c]	
$W_2(TiPB)_2(OSC\text{-}2\text{-}Th)_2$	0.43 ± 0.01[d]		3−10[e]
$W_2(TiPB)_2(O2C\text{-}2\text{-}Th)_2$	0.59 ± 0.01[f]		3−10[e]

[a] λ_{ex} = 514 nm, kinetics monitored at 370 nm. [b] λ_{ex} = 355 nm, kinetics monitored at 600 nm. [c] Inserted from reference 7. [d] λ_{ex} = 675 nm, kinetics monitored at 400 nm. [e] Instrument response limited. [f] λ_{ex} = 675 nm, kinetics monitored at 375 nm.

Transient Absorption Spectroscopy. All four compounds have been examined in THF solutions by both femtosecond (fs) and nanosecond (ns) transient absorption (TA) spectroscopy. The compounds were excited into their ^{1}MLCT bands, and the consequent TA spectra were monitored. The data are summarized in Table 2. All four compounds showed transients with short lifetimes ranging from 400 fs to 4 ps, which we assign to decay of the ^{1}MLCT based S_1 state. It should be noted that the samples of type M_2ThCOS contain a mixture of isomers, as mentioned above, some of which lack a center of inversion. While there is some evidence suggesting the presence of a center of inversion can have a marked effect on the observed dynamics compared to the absence of a center of inversion, the results obtained herein are generally similar (in terms of the number of transient species and decay components observed) to those of homoleptic complexes reported previously[8] which do possess inversion symmetry. Therefore, in these cases, the observed dynamics is an average over all species but there is little effect between the various isomers. The fs TA spectra and the corresponding decay kinetics for **Mo_2ThCOS**, **W_2ThCOS**, and **W_2ThCO$_2$** are depicted in Figure 8, while the ns TA spectrum for **Mo_2ThCOS** is shown in Figure 9. The time-resolved spectroscopic studies on **Mo_2ThCO$_2$** have been recently reported,[7] and the singlet and triplet lifetimes observed for **Mo_2ThCO$_2$** are compared with the rest of the compounds.

One common feature present in the fs TA spectra for each of the studied complexes is the presence of excited state absorption bands belonging to two distinct excited

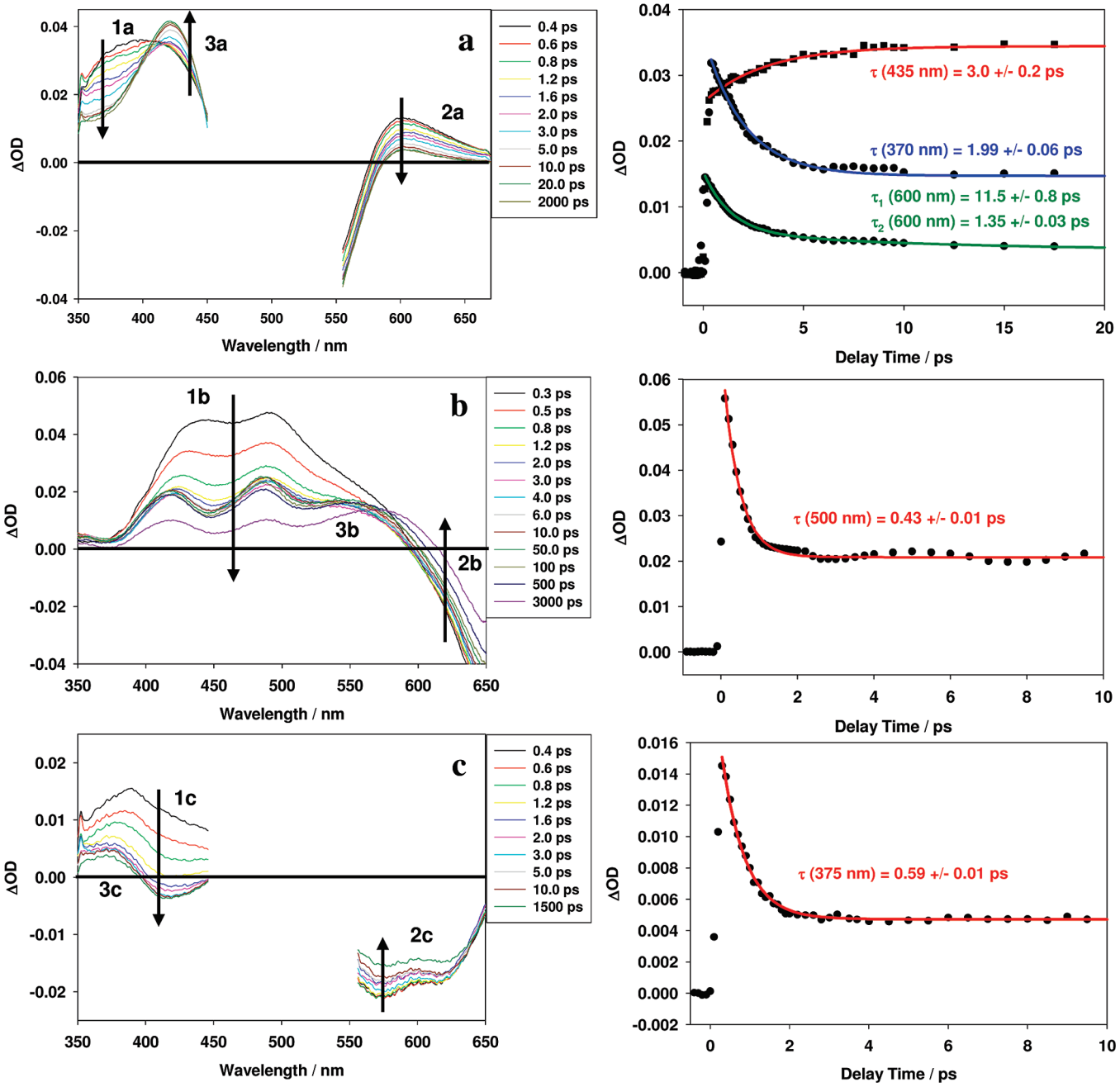

Figure 8. Femtosecond TA spectra (left) and corresponding decay kinetics (right) for compounds (a) **Mo_2ThCOS**, with λ_{ex} = 514 nm; (b) **W_2ThCOS**, with λ_{ex} = 675 nm, and (c) **W_2ThCO$_2$** with λ_{ex} = 514 nm in THF at room temperature.

states. Those bands which are present immediately upon excitation into the ^{1}MLCT absorption and those which persist on the nanosecond time scale or longer are indicative of these states. This is most clearly evident for **Mo_2ThCOS**, as shown in Figure 8, panel a, where bands 1a and 2a are observed directly after excitation but decay to give rise to band 3a. Specifically, bands 1a and 2a decay with lifetimes of ~1.35 and 1.99 ps respectively while band 3a is observed to concurrently grow in on a similar time scale of ~3.0 ps. This result is interpreted as the direct conversion between the singlet and triplet manifolds. Additional kinetics of band 2a should also be noted. Here, both the singlet and triplet states have a positive absorption as indicated by the long time offset in the kinetic trace. A second component to the kinetics is observed, with lifetime ~11.5 ps, and is attributed to vibrational cooling within the triplet state.

The fs TA studies on compound **Mo_2ThCO$_2$** have been previously reported, and it was found that it possessed a short-lived singlet excited state, with lifetime of ~4 ps. The nature of the S_1 excited state was determined to be ^{1}MLCT. This agrees very well with our observations for **Mo_2ThCOS**, and indicates the similarity between these two. The lifetime of S_1 state is found to decrease on going from **Mo_2ThCO$_2$** to **Mo_2ThCOS**.

In the cases of **W_2ThCOS** and **W_2ThCO$_2$**, the excited state absorption bands belonging to the singlet and triplet states are much more convoluted but still distinctly present. Initially for **W_2ThCOS** (Figure 8, panel b), a broad absorption band, 1b, and ground state bleach 2b are

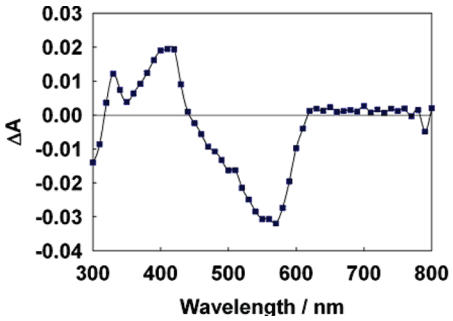

Figure 9. Nanosecond TA spectrum for the compound Mo_2(OSC-2-Th)$_2$(TiPB)$_2$.

observed. Band 1b decays into a more broadened absorption band 3b that covers the same region of the spectrum and is persistent throughout the experiment. Monitoring the kinetics at 500 nm shows an initial decay of 0.43 ps and a much longer component of 2.5 (±1.1) ns. Similarly, **W_2ThCO$_2$** initially possesses the broad absorption band 1c which decays into the narrower, only slightly blue-shifted band 3c. Monitoring the kinetics at 375 nm shows again two components, an initial decay of 0.59 ps and a longer component of 1.0 (±0.5) ns. For both of the tungsten compounds, the short and long-lived components are attributed to the singlet state lifetime and partial ground state recovery from the triplet state, respectively. Additionally, the recovery of the MLCT bleach with lifetimes similar to the aforementioned long components supports the assignment as the process converting the triplet state to the ground state. Overall, changing the metal center leads to a significant reduction in both the singlet and triplet state lifetimes.

ns TA also revealed the presence of longer lived transients, which are assigned to triplet states. The ns TA spectra for the dimolybdenum compound **Mo_2ThCOS** is shown in Figure 9 while that for the recently reported **Mo_2ThCO$_2$**[7] is shown in Supporting Information, Figure S6. It is worthy of note that the TA spectra corresponding to the two molybdenum compounds are very similar, and the triplet excited states possess comparable lifetimes, in the range of ~50−70 μs. Lifetimes of the triplet excited states of the ditungsten compounds, **W_2ThCOS** and **W_2ThCO$_2$**, could not be accurately determined from their ns TA measurements because of instrument limitations (fwhm ~ 8 ns). However fs TA measurements have revealed the presence of a long-lived excited state in both **W_2ThCOS** and **W_2ThCO$_2$** with lifetimes of 1−2.5 ns (vide supra).

The two excited states observed in the fs TA experiments are also consistent with the emissive nature of each of the complexes. **Mo_2ThCO$_2$** is dual emissive and the luminescent states are correlated with the singlet and triplet states observed in the TA experiments. However, in **Mo_2ThCOS**, the −COS functionality provides better coupling to the metal center, reducing the singlet state lifetime to ~2 ps, and, consequently, the MLCT fluorescence is weaker. Similarly, **W_2ThCO$_2$** exhibits very weak fluorescence and has a longer singlet state lifetime (~0.59 ps) than **W_2ThCOS** (~0.43 ps), which possesses only one emissive state.

The dynamics observed in the triplet state bands and in the ns TA experiments can also be correlated to the lower energy emission for each of the complexes in the NIR. For the Mo_2 containing complexes, the triplet state lifetimes are too long (see below) to be estimated in the fs TA experiment. However, Figure 8a shows that the TA signal does not return to the baseline, consistent with the presence of a long-lived state. The long-lived T_1 states correspond to the ^{3}MM$\delta\delta^*$ states, which decay radiatively by emitting at ~1100 nm. These emissions were solvent independent and showed vibronic features at 77 K, corresponding to υ(MoMo) stretching mode (See Supporting Information, Figure S3).

On the basis of the observation from the combined TA studies, it can be concluded that both **W_2ThCOS** and **W_2ThCO$_2$** possess triplet excited states, which evolve upon direct intersystem crossing from the singlet excited state. The short lifetimes of these T_1 states (3 −20 ns) and the energy of emission from the T_1 states unequivocally points to them being ^{3}MLCT based. As can be seen from Table 2, the T_1 lifetimes for tungsten are notably shorter than for molybdenum even though they could not be accurately determined. The lifetimes of triplet states also increase on going from **Mo_2ThCOS** to **Mo_2ThCO$_2$**. This is consistent with the introduction of the heavier element, W versus Mo and S versus O, which introduces greater spin−orbit coupling. Also, the lower energy of T_1 states with the heavier elements enhances non-radiative decay.

Concluding Remarks

The effect of substitution of S for O in the carboxylate linker has a pronounced effect on the electro-optical properties of these compounds. Notably the ^{1}MLCT is red-shifted and the redox potentials are also affected as a result of stabilization of the $M_2\delta$ orbital. The latter effect is offset for molybdenum because the S 3p and Mo_2 δ orbitals are close in energy leading to a filled−filled orbital interaction which compensates for the enhanced back-bonding. The replacement of an O by S in the $-O_2C$ moiety also decreases the lifetimes of the S_1 states, presumably because of enhanced spin-orbit coupling which facilitates intersystem crossing. A notable difference between molybdenum and tungsten is seen in the nature of T_1 states that we assign to ^{3}MoMo$\delta\delta^*$ and ^{3}WLCT. For tungsten, the ^{3}WLCT states have lifetimes between 3 and 20 ns, which are notably shorter than the 1.6 μs for the ^{3}WW$\delta\delta^*$ of W_2(TiPB)$_4$.[8]

Experimental Section

Measurements. NMR spectra were recorded on a 400 MHz Bruker DPX Advance400 spectrometer. All ^{1}H NMR chemical shifts are in ppm relative to the protio impurity in THF-d_8 at 3.58 ppm.

Electronic spectra at room temperature were recorded using a Perkin-Elmer Lambda 900 spectrometer in THF solution. A 10.00 mm IR quartz cell was employed.

The cyclic voltammogram and differential pulse voltammogram of all the complexes were collected at a scan rate of 100 mV s^{-1} and 5 mV s^{-1}, respectively, using a Princeton Applied Research (PAR) 173A potentiostat-galvanostat equipped with a PAR 176 current-to-voltage converter. Electrochemical measurements were performed under an inert atmosphere in a 0.5 M solution of ^{n}Bu$_4$NPF$_6$ in THF inside a single compartment voltammetric cell equipped with a platinum working electrode, a platinum wire auxiliary electrode, and a pseudoreference electrode consisting of a silver wire in 0.5 M ^{n}Bu$_4$NPF$_6$/THF separated from the bulk solution by a Vycor tip. The potential

values are referenced to the $FeCp_2/FeCp_2^+$ couple, obtained by addition of a small amount of $FeCp_2$ to the solution.

Nanosecond TA measurements were carried out in 1 × 1 cm square quartz cuvettes equipped with Kontes stopcocks. Nanosecond TA spectra were measured on a home-built instrument pumped by a frequency doubled (532 nm) or tripled (355 nm) Spectra-Physics GCR-150 Nd:YAG laser (fwhm ~ 8 ns, ~ 5 mJ per pulse). The signal from the photomultiplier tube (Hamamatsu R928) was processed by a Tektronics 400 MHz oscilloscope (TDS 380).[16]

The steady-state NIR-luminescence measurements at 77 K were carried out in J. Young NMR tubes. The spectra were measured on a home-built instrument utilizing a germanium detector. The sample was excited at 658 nm (laser diode max power: 65mW), and a RG830 long pass filter was placed between the sample and the detector.

The femtosecond TA experiments were carried out using laser and detection systems that have been previously described.[17] The samples were prepared with absorbance ~0.4−0.8 at the excitation wavelength and were excited at 675 nm for $W_2(TiPB)_2(O_2C\text{-}2\text{-}Th)_2$ and 514 nm for $Mo_2(TiPB)_2(OSC\text{-}2\text{-}Th)_2$ and $W_2(TiPB)_2(OSC\text{-}2\text{-}Th)_2$ (with excitation power ~ 1−2 μJ at the sample). During the measurements, the samples were kept in constant motion by manual movement of an *XYZ* stage in the vertical and horizontal directions. To ensure that no photodecomposition occurred during data collection, absorption spectra were recorded before and after the TA measurements. The measurements were repeated four times at each of the pump−probe delay positions to confirm data reproducibility throughout the experiment, and the resulting spectra were corrected for the chirp in the white-light super continuum.[18] The kinetics were fit in general to a sum of exponential decay terms of the form, $S(t) = \sum_i A_i \exp(-t/\tau_i) + C$ or to an exponential rise to maximum of the form $S(t) = A_i(1 - \exp(-t/\tau)) + C$, with amplitude, A_i, lifetime, τ, and offset, C, using Origin 6.0. Error bars for the lifetimes are reported as the standard error of the exponential fit.

Microanalysis was performed by H. Kolbe Microanalytisches Laboratorium, Germany.

MALDI-TOF was performed on a Bruker Reflex III (Bruker, Bremen, Germany) mass spectrometer operated in a linear, positive ion mode with an N_2 laser. Dithranol was used as the matrix and prepared as a saturated solution in THF. Allotments of matrix and sample were thoroughly mixed together; 0.5 mL of this was spotted on the target plate and allowed to dry.

All reactions were carried out under one atmosphere of oxygen-free UHP-grade argon using standard Schlenck techniques or under a dry and oxygen-free nitrogen atmosphere using standard glovebox techniques. All manipulations of the studied compounds were performed in a nitrogen-filled glovebox or by using standard Schlenck line techniques in an atmosphere of oxygen-free UHP-grade argon. All solvents were dried over the appropriate drying agent, distilled prior to use, and stored in reservoirs equipped with Kontes taps over activated 4 Å molecular sieves, under an argon atmosphere and degassed prior to use.

The starting materials $Mo_2(TiPB)_4$[19] and $W_2(TiPB)_4$[20] were prepared according to published procedures. The compounds $M_2(TiPB)_2(ThCO_2)_2$, where M = Mo or W were also synthesized according to reported procedures.[6]

Synthesis of 2-Thiophenecarbothioic Acid ($C_5H_4OS_2$ = ThCOSH). 2-Thenoyl chloride (0.15 mL, 1.4 mmol) was dissolved in dry benzene and then added dropwise to a suspension of thioacetamide (0.13 g, 1.7 mmol) in benzene. This was then stirred at 35 °C for 3 h after which an equal volume of 10% KOH (w/w) was added to it. This was allowed to stir for another 30 min. After separating the two layers, dil. HCl acid was added to the aqueous layer. The organic droplets were extracted with CH_2Cl_2 and then evaporated. The oily liquid was used in situ for the next step.

Synthesis of $Mo_2(TiPB)_2(OSC\text{-}2\text{-}Th)_2$. $Mo_2(TiPB)_4$ (0.62 g, 0.5 mmol) was dissolved in dry toluene and then added to the ThCOSH acid (0.14 g, 1 mmol) in situ. The suspension was stirred at room temperature for 3 days, at the end of which an intense pink precipitate had formed. This was centrifuged and washed with toluene (2 × 10 mL) before being dried in vacuo to give 350 mg (72% yield) of a pink solid. Microanalysis found: C 51.81, H 5.34 $C_{42}H_{52}Mo_2O_6S_4$ requires: C, 51.84; H, 5.39. NMR (THF-d_8): δ_H (400 MHz) 8.63 (d, 2H, J_{HH} = 4 Hz), 7.69 (d, 2H, J_{HH} = 4 Hz), 7.21 (d, 2H, J_{HH} = 4 Hz), 7.05 (s, 4H), 3.20 (m, 4H), 2.97 (m, 2H), 1.28 (d, 12H, J_{HH} = 7 Hz), 1.14 (d, 24H, J_{HH} = 7 Hz) ppm. MALDI-TOF: Calculated monoisotopic MW for $C_{42}H_{52}Mo_2O_6S_4$: 973.0. Found: 970.91 (M^+). UV−vis−NIR (in THF, 293 K, values of ε (M^{-1} cm^{-1}) are given in parentheses): 545 (~10000), 510 (~11000), 290 (~20000) nm.

Crystallographic Data. Space group: $P2_1/c$. Unit cell dimensions: a = 10.936(1)Å, b = 14.124(1)Å, c = 17.096(2)Å, β = 97.318(3)°.

Synthesis of $W_2(TiPB)_2(OSC\text{-}2\text{-}Th)_2$. $W_2(TiPB)_4$ (0.15 g, 0.12 mmol) was dissolved in dry toluene and then added to the ThCOSH acid (0.288 g, 0.20 mmol) in situ. The suspension was stirred at room temperature for 5 days, at the end of which a blue precipitate had formed. This was centrifuged and washed with toluene (2 × 10 mL) before being dried in vacuo to give 103 mg (75% yield) of a blue solid. Microanalysis found: C 43.84, H 4.49 $C_{42}H_{52}W_2O_6S_4$ requires: C, 43.91; H, 4.56. NMR (Benze ne-d_6): δ_H (400 MHz) 7.60 (d, 2H, J_{HH} = 4 Hz), 6.96 (s, 4H), 6.76 (d, 2H, J_{HH} = 4 Hz), 6.68 (d, 2H, J_{HH} = 4 Hz), 3.11 (m, 4H), 2.76 (m, 2H), 1.30 (d, 12H, J_{HH} = 7 Hz), 1.19 (d, 24H, J_{HH} = 7 Hz) ppm. MALDI-TOF: Calculated monoisotopic MW for $C_{42}H_{52}W_2O_6S_4$: 1148.8. Found: 1148.0 (M^+). UV−vis-NIR (in THF, 293 K, values of ε (M^{-1} cm^{-1}) are given in parentheses): 720 (~23000), 665 (~17000), 390 (~7000), 300 (~13000) nm.

Theoretical Approaches. Electronic structure calculations on the model compounds were performed by DFT[11−14] with the aid of the Gaussian03[21] suite of programs. The B3LYP[22,23] exchange correlation functional was used along with the 6-31G* basis set for C, H, and O, 6- 31+G (2d) basis set for S, and the SDD energy consistent pseudopotentials for molybdenum and tungsten. Geometry optimizations were performed in

(16) Byrnes, M. J.; Chisholm, M. H.; Gallucci, J. A.; Liu, Y.; Ramnauth, R.; Turro, C. *J. Am. Chem. Soc.* **2005**, *127*, 17343.
(17) Burdzinski, G.; Hackett, J. C.; Wang, J.; Gustafson, T. L.; Hadad, C. M.; Platz, M. S. *J. Am. Chem. Soc.* **2006**, *128*, 13402.
(18) Nakayama, T.; Amijima, Y.; Ibuki, K.; Hamanoue, K. *Rev. Sci. Instrum.* **1997**, *68*, 4364.
(19) Cotton, F. A.; Hillard, E. A.; Murillo, C. A.; Zhou, H.-C. *J. Am. Chem. Soc.* **2000**, *122*, 416.
(20) Santure, D. J.; Huffman, J. C.; Sattelberger, A. P. *Inorg. Chem.* **1985**, *24*, 371.
(21) Frisch, M. J.; Trucks, G. W.; Schlegel, H. B.; Scuseria, G. E.; Robb, M. A.; Cheeseman, J. R.; Montgomery, Jr., J. A.; Vreven, T.; Kudin, K. N.; Burant, J. C.; Millam, J. M.; Iyengar, S. S.; Tomasi, J.; Barone, V.; Mennucci, B.; Cossi, M.; Scalmani, G.; Rega, N.; Petersson, G. A.; Nakatsuji, H.; Hada, M.; Ehara, M.; Toyota, K.; Fukuda, R.; Hasegawa, J.; Ishida, M.; Nakajima, T.; Honda, Y.; Kitao, O.; Nakai, H.; Klene, M.; Li, X.; Knox, J. E.; Hratchian, H. P.; Cross, J. B.; Bakken, V.; Adamo, C.; Jaramillo, J.; Gomperts, R.; Stratmann, R. E.; Yazyev, O.; Austin, A. J.; Cammi, R.; Pomelli, C.; Ochterski, J. W.; Ayala, P. Y.; Morokuma, K.; Voth, G. A.; Salvador, P.; Dannenberg, J. J.; Zakrzewski, V. G.; Dapprich, S.; Daniels, A. D.; Strain, M. C.; Farkas, O.; Malick, D. K.; Rabuck, A. D.; Raghavachari, K.; Foresman, J. B.; Ortiz, J. V.; Cui, Q.; Baboul, A. G.; Clifford, S.; Cioslowski, J.; Stefanov, B. B.; Liu, G.; Liashenko, A.; Piskorz, P.; Komaromi, I.; Martin, R. L.; Fox, D. J.; Keith, T.; Al-Laham, M. A.; Peng, C. Y.; Nanayakkara, A.; Challacombe, M.; Gill, P. M. W.; Johnson, B.; Chen, W.; Wong, M. W.; Gonzalez, C.; Pople, J. A. *Gaussian03*; Gaussian, Inc.: Wallingford, CT, 2004.
(22) Becke, A. D. *Phys. Rev. A: Gen. Phys.* **1988**, *38*, 3098.
(23) Miehlich, B.; Savin, A.; Stoll, H.; Preuss, H. *Chem. Phys. Lett.* **1989**, *157*, 200.

appropriate symmetry and were confirmed as local minima on the potential energy surfaces using frequency analysis. Orbital analyses were performed using Gaussview.[15]

Acknowledgment. We thank the National Science Foundation for support of this work through NSF CHE0515835, and we also thank the Institute of Materials Research at The Ohio State University for partial support of this work. The Ohio Supercomputing Center is acknowledged for providing computational resources. We also acknowledge Dr. Judith Gallucci for examining the crystals of **Mo_2ThCOS**.

Supporting Information Available: Listings of preliminary ORTEP plot for **Mo_2ThCOS**, variable temperature absorption spectra for **W_2ThCO_2**, NIR emission spectra for **Mo_2ThCOS**, ns TA spectra for **Mo_2ThCO_2**, and Gaussview plots of frontier orbitals for model compounds. This material is available free of charge via the Internet at http://pubs.acs.org.